System Architecture for De-orbiting Spacecrafts as a Platform for Experimental Aerodynamics Studies

Nandeesh Hiremath
Assistant Professor
Department of Aerospace Engineering
California Polytechnic State University
1 Grand Ave, San Luis Obispo, CA
nhiremat@calpoly.edu

Justin Self
Department of Aerospace Engineering
California Polytechnic State University
1 Grand Ave, San Luis Obispo, CA
jtself@calpoly.edu

Nathan Eller
Department of Aerospace Engineering
California Polytechnic State University
1 Grand Ave, San Luis Obispo, CA
neller@calpoly.edu

***Abstract*—Space vehicles encountering the Earth's atmosphere are enveloped in a shock layer comprising an intense bow shock, further trailing into a shallow oblique shock. Due to remarkably high flight speeds approaching near orbital velocities, the detached shock layer heats the air, resulting in immense velocity and temperature gradients. Between the shock and the vehicle, there are velocity, thermal, entropy, and chemical boundary layers that are not self-similar. The shock detachment distance is inversely proportional to the Mach number, and at hypersonic speeds, the boundary layer thickness and shock layer are in juxtaposition. The vastly dominant flow regime surrounding the bodies of arbitrary shapes like orbital debris, rogue de-orbiting spacecraft, or meteoroids is a matter of great interest in accurately predicting their flight path. The forces derived from onboard inertial measurement units may not be accurate in predicting the flight path and ground footprint of disintegrating spacecraft. Predictions requiring accurate aerodynamic characterization mandate high-fidelity simulations, which in turn require prior experimental validations. More often than not, in dynamically evolving situations like the disintegrating spacecraft, the predictions are heavily reliant on reduced-order models that are incidentally successful. As for the existing ground test facilities, they are designed to respect only a small set of flow similarity parameters at a time. These are often short-duration test facilities, ranging from milliseconds to a few seconds per test, and the runtime costs limit the operational frequencies. More recently, small spacecraft have been proposed as an inexpensive alternative to ground test facilities. Although limited in their payload capacity to accommodate a vast number of sensors and limited in controllability and repeatability, these provide actual in-flight measurements.**

The current research is focused on exploring the viability of small spacecraft for obtaining aerodynamic characterization for atmospheric re-entry. This paper will provide a system architecture for a) direct aerodynamic load measurement from a de-orbiting spacecraft, b) scientific missions to characterize aerodynamic loads for bodies of arbitrary shapes, and c) small spacecraft as a viable alternative platform for experimental aerodynamics research. The study brings in perspectives on challenges and opportunities in utilizing the small spacecraft as a platform to investigate complex aerodynamic phenomena. This will be followed by the exploration of viable flight path envelopes for scientific missions carrying payloads for aerodynamic studies and the assessment of the impact on ground footprints of disintegrating rogue spacecraft due to uncertainty in aerodynamic and geometric parameters. Lastly, the study proposes the use of an array of micro-electromechanical pressure sensors to directly measure unsteady aerodynamic forces from bodies of arbitrary shapes subjected to arbitrary flight attitudes. Such a measurement system integrated into small spacecraft would provide better insights into dynamically evolving flow characteristics than the integrated forces deduced from inertial measurement systems. The scope is limited to the integration of a pressure sensor array using open-source embedded systems, followed by assessing system performance and limitations.

979-8-3503-0462-6/24/$31.00 ©2024 IEEE

TABLE OF CONTENTS

1. INTRODUCTION

Bluff body aerodynamics is a topic of broader interest. Conventional aerodynamics is suitable for studying atmospheric flight systems, which are typically streamlined. Outside the very small range of very low-subsonic Mach numbers, the closed-form solutions do not extend to complex shapes and flow regimes. The bluff bodies have vastly complex flow regimes, resulting in 3D flow features as shown in Figure 1 and references [1–10]. There is extensive literature available for a few canonical 2D shapes. However, the extrapolated [11] results do not conform to the three-dimensional geometries. The existing prediction capabilities are based on physics-based computational tools that solve Navier-Stokes equations. Several 3D phenomena like sharp-edge vortex and three-dimensional large-scale vortices are not captured [12]. Such features are sensitive to the chosen turbulence models and may often be missed due to manual grid refinement. Experimental measurements are needed to calibrate the models, but the major challenge is to replicate the actual flight environment. Several wind tunnel facilities worldwide focus on replicating the flow physics by respecting, at most, only a couple of dynamic similarity parameters. Such ground

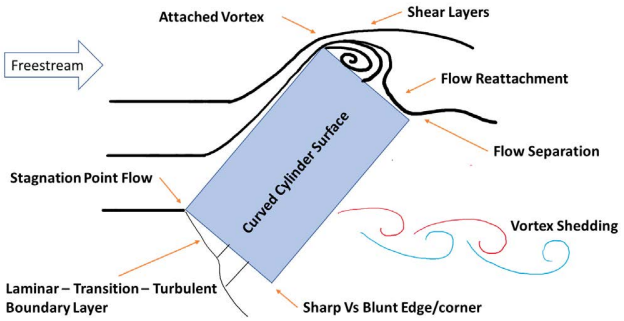

Figure 1: **Finite aspect ratio cylinder in yaw in subsonic flow showing several observable flow features that are strongly influenced by edges, corners, and roughness. Such features appear at shorter spatial and temporal scales for hypersonic speeds.**

test facilities are uniquely designed to study a very narrow region of the re-entry flight envelope. Such an approach is economically not viable for studying a vast variety of 3D shapes. The authors propose the actual flight test measurements for targeted (re)entries as a viable alternative. This paper explores the possibility of using re-entering spacecraft to measure the aerodynamic and thermal loads. Specifically, it addresses the small spacecraft as an alternative to wind tunnel testing and simulations by complementing targeted flight test measurements.

Bluff bodies come in various forms with complex flow phenomena at various attitudes. Mapping the air loads on bluff bodies at arbitrary orientations in itself has scientific merit. This vastly unexplored area of aerodynamics was not of significance in the development of aerodynamic theory as the primary objective of the time was confined to lift generation from streamlined objects [13, 14]. However, the scenario is changing with more focus on space architectures for atmospheric (re)entry missions that are not necessarily streamlined. Because of the rarefied environment typically seen in the upper atmospheres, the aerodynamic forces will be negligible. As the spacecraft (re)enters the atmosphere, a denser atmosphere is encountered, contributing to measurable aerodynamic forces. These spacecraft modules are primarily ballistic (re)entry systems, except for a few concepts like hypersonic glide vehicles and space shuttles that use aerodynamic lift. Our current focus is on the ballistic (re)entry modules, which come in various shapes, from pointy noses to cuboidal shapes. Specifically, small spacecraft like CubeSats and NanoSats have gained prominence in academic and scientific missions due to their cheaper costs and simpler architecture. Owing to their modularity, they can be prime platforms for aerodynamic investigations. Complementing the ground-based wind tunnel testing, such flight testing will take prominence in the fast-evolving space sector. While small spacecraft missions have gained prominence over the past couple of decades, there are still red flags about their success rates. More often than not, they fail prior to or during launch. Most of these systems were developed within academia as cheaper platforms to educate students on spacecraft dynamics; reliability of the mission was not the primary goal. With the inculcation of systems engineering and mission architecture within the aerospace curriculum across the universities, the reliability of small spacecraft is expected to be much better. Also, a thriving private sector is building constellations of large and small spacecraft for terrestrial and interplanetary scientific missions and telemetry.

Figure 2: **Orbital debris encountering hypersonic to subsonic flight regime. Courtesy: ESA-D Durcos.**

Within the (re)entry corridor or the flight path envelope, the spacecraft decelerates from planetary approach (hypersonic) velocities to subsonic speeds. These spacecraft modules experience drastic changes in flow field from rarefied to continuum flows over several passes. The (re)entry trajectories are predictable through telemetry and oftentimes deviate from the said course due to continuous disintegration from aerodynamic heating, except for reusable modules. The orbit parameters and (re)entry points deviate from the set parameters during the launch phase, primarily due to dynamically changing atmospheric conditions and faulty systems during the tail end of the missions. Owing to these uncertainties posed by nature, the engineering solutions can be thought of along two avenues.

(A) Ground and space-based optical telemetry for continually tracking the modules has been prevalent. These existing systems are subject to clear weather conditions and are limited to pre-planned flight paths. Ground (and sea-based) telescopes are often spatially limited to high-altitude regions with clear weather. It clearly is not a viable solution for targeted (re)entry. In Section 3, we propose an aerial-based approach using high-altitude fixed-wing systems for targeted (re)entries. Incidentally, targeted (re)entry has not been in the mainstream, and there is a huge opportunity for technology development that can be used for multi-spectral imaging of spacecraft. This high-altitude aerial platform flying above the cloud layers and devoid of jet streams can be used for wildfire detection (looking down) and deep space observations (looking up).

(B) Secondly, complementing the optical tracking systems; currently, the onboard systems continually update the forces experienced by the spacecraft through inertial measurement units (IMU) and either recorded on board (retrieved upon ground impact) or relayed to ground stations. The accelerations and moment of inertia are further used to deduce the derived quantities like aerodynamic forces, flight velocity, and flight path. There have been reported flight test aerodynamic data that show huge deviations of these derived quantities from the computationally predicted results (Direct Simulations Monte Carlo for free molecular flows, Reynolds Averaged Navier-Stokes Solvers for continuum flows). Such comparisons can only be achieved for successful retrieval

of the data, mostly upon ground impact. Almost all small spacecraft are designed to burn during atmospheric (re)entry caused by aerodynamic heating. In such a scenario, purely relying on the inertial measurements for a disintegrating spacecraft (Figure 2) might not be a viable approach. The proposed framework in Section 4 provides an avenue to gather aerodynamic flow properties at sufficient spatial and temporal resolution, in addition to the aerial optical tracking capability. This framework opens a huge opportunity for scientific missions catered toward bluff body aerodynamics. The disagreement between the flight test aerodynamic data and computationally predicted aerodynamic loads shows the inherent limitations of the state-of-the-art tools wherein physical phenomena might not be captured due to sensitivity to chosen models (turbulence, free molecular) or manual grid refinement practices. Small spacecraft platforms can be the *future flying wind tunnels*, enabling direct flight measurements while surpassing the difficulty of replicating flight parameters in ground test facilities.

Prior Work

Bluff Body Aerodynamics: In the recent past, the authors have developed a Continuous Rotation Technique (CRT) [15–24] that enables measuring all 6 DOF air loads on finite aspect ratio bodies for low-speed flows under quasi-steady conditions. Such a capability is installed at California Polytechnic State University, San Luis Obispo's $3ft \times 4ft$ Low Speed Wind Tunnel (Cal Poly LSWT) [25]. Prior to this work, the experimentally measured datasets were limited to Hoerner's [26, 27] 2D configurations [28], and a select 3D shapes [29–35] as part of helicopter slung load certifications. Air loads measured using CRT about the orthogonal axes are further used in estimating the forces and moments about any arbitrary orientation based on vector decomposition [36]. This approach has been very successful in testing a vast number of 40+ canonical shapes and practical shapes in a short period of time. All the air loads are depicted as 20-term Fourier coefficients, making them easily deployable to various design tools. These integrated air loads obtained from load cells show the presence of side forces caused by a sharp-edge vortex observed along the side surface of a circular cylinder. This is contrary to the notion of shed vortices [37]. Static pressure measurements [38] have shown suction pressures on the leeward side of the cylinder, showing an indication of vortex-induced lift contributing to the side force generation. This led the curiosity to venture into developing a wireless pressure sensor system that can be used for bluff body studies, not limited to quasi-steady flow conditions [39, 40] with applications to flow control [41–43]. This system is currently being designed and developed for low-speed wind tunnel testing with the interest of understanding subsonic flow fields behind a normal shock. The proposed architecture, owing to its modularity and relatively good sampling rates, can be implemented directly on small spacecraft' scientific payloads for aerodynamic studies. Conventional approaches with similar scientific payloads are geared toward studying flight mechanics [44], atmospheric conditions, and rudimentary flow characteristics. We are proposing a small spacecraft as an alternative testing platform for studying bluff body aerodynamics.

Flight Test: The flight test data from Adaptable Deployable Entry and Placement Technology (ADEPT) [45] shows that the heat shield, which is primarily a bluff object, undergoes higher rotation rates [46] about the roll axis than what was predicted computationally. Such behavior is observed after 350 seconds of flight time when the module was decelerated to less than Mach 0.5. This technology demonstrator showed the imminent need for resolving bluff body features encountered during actual flight. The inertial measurements corroborated with the ambient weather balloon data are the only sources for calculating the integrated forces and rotation rates. Most of the finer details like surface pressure distribution were estimated *a priori* using computational tools with pertinent models for free-molecular to continuum flows. The sub-scale wind tunnel testing [47] underestimated the roll rates. While the sub-scale model was designed to achieve the stated objectives of their research, the lower mass moments and products of inertia coupled with aerodynamic effects could be the limiting factor. In recent years, the ESA's Qarman CubeSat developed at von Kàrmàn Institute [48–50] was aimed at studying the reentry flow physics (not bluff body aerodynamics); however, the mission was not quite successful as the CubeSat took a longer trajectory before entering the Earth's atmosphere. The primary cause was possibly attributed to insufficient modeling of prolonged solar exposure resulting in communication blackout. It is expected that such efforts will increase in the future. An aerodynamic testing platform using small spacecraft can be a viable approach to providing direct flight test data, wherein the modularity of the system can be exploited in sweeping through several shapes and sizes.

Aerial Optical Diagnostics: Continuous data relay to the ground station and GPS tracking is a crucial component for flight tests. The number of satellites and their coverage area limit the positional and velocity resolution. It is evident that several uncertainties in the launch window and delays during phase separations can result in slightly different flight trajectories, which may not be picked up by the satellites as intended [45]. A targeted (re)entry flight test platform is much needed. Regarding bluff body aerodynamics, space-based observations have limited viewing angles in capturing the underside of the (re)entry modules where most of the phenomena happen. Ground or sea-based observatories like Atacama Cosmology Telescope [51] cannot be used for targeted (re)entry studies. Tropospheric aerial approaches like NASA's Hypersonic Thermodynamic Infrared Measurements (HYTHIRM) [52–54] performed from US Navy NP-3D aircraft flown at the edge of the troposphere (aircraft ceiling altitude is 31,000 ft) mandate clear weather conditions. These limitations can be circumvented by using high-altitude aerial platforms using a swarm of fixed-wing unmanned aircrafts. Komerath *et. al.* [55–60] have shown that a high-altitude fixed-wing aircraft in swarm configurations is more feasible and much needed for reversing global warming, wherein reflective sheets from the canopy of the aircraft reflects away a portion of solar radiation. We propose to use these high-altitude aircraft for multi-spectral imaging of (re)entering spacecraft. It is shown that the estimated magnification and irradiating intensity observed from these high-altitude aircraft are capable of resolving terrestrial features, importantly wild-fire detection [61]. The present work builds upon our prior studies [62–64] on *Virtual Aperture* of the size of Pacific Ocean to obtain several orders of magnitude improvements in image resolution for studying the underside of (re)entering spacecraft.

2. SYSTEM ARCHITECTURE

Figure 3 shows the concept of operation for using small spacecraft as a platform for studying bluff body aerodynamics in tandem with high-altitude fixed-wing aircraft for multi-spectral imaging of the reentering spacecraft. A swarm of high-altitude aircraft are flown along the west coast of the

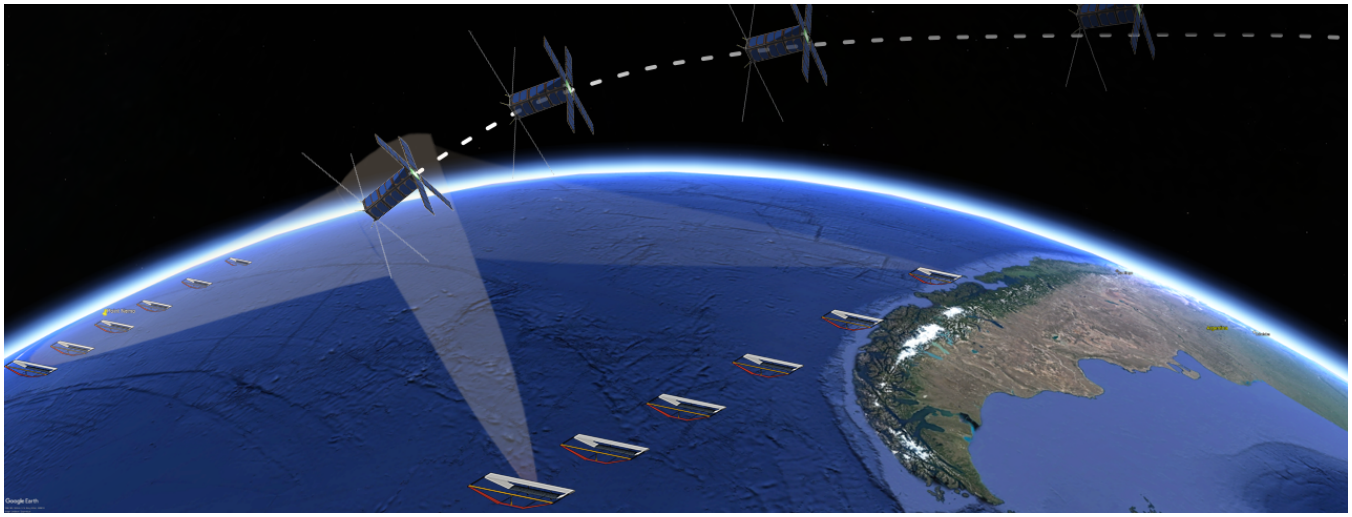

Figure 3: **Concept of operation showing (A) high altitude multi-spectral imaging capability followed by (B) reentering CubeSat as a test bed for bluff body aerodynamics studies. This scalable architecture targets the unexplored technology space for exploiting targeted reentry.**

Americas and the east coast of Japan, providing a *Virtual Aperture* the size of the Pacific Ocean. This flight path is particularly chosen to maximize the encounters with de-orbiting spacecraft crashing at Point Nemo. These systems are maneuverable and could be deployed wherever targeted reentry is expected, e.g. the Indian Ocean; another popular de-orbit zone. Or they can be deployed at short notice to track rogue deorbiting spacecraft that are not in the coverage area of the satellites. This section explores the flight environment experienced by a de-orbiting spacecraft, starting from its Earth approach point to ground impact. The *Virtual Aperture* capabilities are discussed with perspectives on the estimated magnification and irradiation. Subsequently, in Section 4, we explore the wireless pressure measurement system.

Flight Envelope Reentry Characteristics

Trajectories— In order to assess the design space for the onboard pressure and temperature ranges/sensitivities and the expected irradiation intensity at observing altitudes, the expected ambient and flight characteristics for ballistic entry small spacecraft are essential. Accurate estimates of impact location(s) and ground footprints of reentry objects and any associated debris fields are of vital importance to the safety of people on the ground whose locations may be near reentry groundtrack pathways. Current reentry predictive models are accurate to less than a day, but uncertainties in predictions still abound. Orbital perturbations due to a non-spherical Earth present a problem in determining the spacecraft's final location of demise, but further challenges present themselves. Accurately predicting current atmospheric models of the flight path envelope is further complicated due to constantly fluctuating upper atmosphere densities as a result of solar wind and magnetic field disturbances. All these parameters, and more, contribute to difficulty in reentry predictions.

Targeted reentry, or controlled reentry, is rare among all orbital reentry events, but targets are often directed to burn up over remote areas, as illustrated in Figure 4. Typically targeted reentry trajectories are required for spacecraft that contain components or materials that have a high probability of not fully burning up during reentry and may impact the ground. In these cases, a ground or high-altitude optical sensing system may be able to capture hypersonic flow phenomena in NIR or IR bands, for instance. Tracking the trajectories and planned reentry zones for these (usually) larger spacecraft would be vital for the imaging team to prepare well in advance for the incoming target. With advances in orbital reentry prediction models and the potential to study reentry objects using high-mobility imaging systems at high altitudes, the feasibility of obtaining high resolution data of hypersonic flow in the near future seems promising.

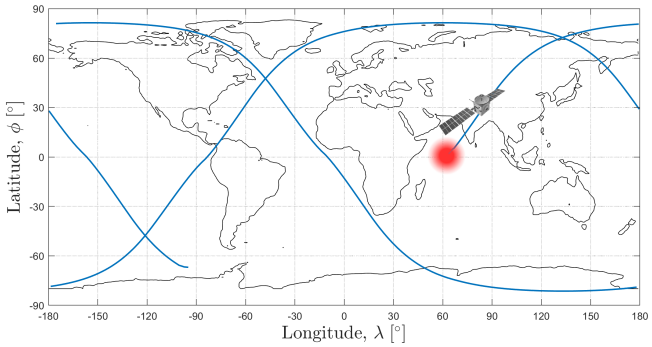

Figure 4: **Example groundtrack for a small satellite that deorbits over the Indian Ocean, a popular targeted reentry location due to its remote location.**

Predicted Reentry Characteristics— Starting with a hypersonic reentry at 100 km altitude and a tumbling 1U Cubesat, some flight reentry characteristics can be parameterized. Assuming the well-documented drag coefficient for a "de-orbiting spacecraft" of 2.22, yet taking into consideration the reasonable maximum 3-σ uncertainty of 20% as [46] outlines, baseline stagnation temperatures, pressures, Mach, and velocity plots can be developed, shown in Figures 5 and 6.

For a non-lifting body, the velocity reentry envelope part of Figure 5 can be calculated by considering the weight vector (W) , lift (not accounted for for ballistic reentry), drag (D), with respect to the relative freestream velocity (V). Taking the small angle approximation ($\theta \approx 0$) for flight path angles

(as is the case for most reentry applications) and rearranging terms:

$$W sin\theta - D = m\frac{dV}{dt}$$

$$-D = \frac{W}{g}\frac{dV}{dt}$$

The drag term, D, can be expressed in terms of the drag coefficient, C_D as $D = \frac{1}{2}\rho V^2 S C_D$, where ρ is freestream density and S is reference area. Thus, we obtain:

$$-\frac{1}{g}\frac{dV}{dt} = \left(\frac{W}{C_D S}\right)^{-1}\frac{\rho V^2}{2} \tag{1}$$

Numerical integration of (1) was performed using the standard Runge-Kutta ODE solver `ode45` in `MATLAB` and was plotted against altitude. Three standard deviations in C_D were plotted to simulate a tumbling spacecraft and/or breakup.

The Mach/Altitude profile for a 1U deorbiting CubeSat was calculated using thermally perfect gas equations by accounting for the vibrational modes under thermal equilibrium conditions. Real gas effects and non-equilibrium chemical kinetics at high-altitude hypersonic conditions are beyond the scope of our current work.

$$a^2 = RT\left(1 + \frac{\gamma_{perf} - 1}{1 + (\gamma_{perf} - 1)\left(\frac{\Theta}{T}\right)^2 \frac{exp^{\Theta/T}}{(exp^{\Theta/T} - 1)^2}}\right) \tag{2}$$

Where a is the speed of sound,γ is a function of static temperature, T, the characteristic vibrational mode temperature for air $\Theta = 3056$K, and R is the real gas constant for air.

Isentropic relations in freestream conditions were used to obtain the total pressure and temperature at a given altitude ash shown in Equations. (3) and (4). Stagnation pressures *at the front* of the deorbiting CubeSat, shown in Figure 6, were found by solving normal shock relations corrected for vibrational modes.

$$\frac{P}{P_t} = \left(\frac{T}{T_t}\right)^{\frac{\gamma}{\gamma-1}} \tag{3}$$

$$\frac{T}{T_t} = \left(1 + \frac{\gamma - 1}{2}M^2\right)^{-1} \tag{4}$$

$$\frac{P_{t_1}}{P_{t_0}} = \left(\frac{(\gamma+1)M^2}{(\gamma-1)M^2 + 2}\right)^{\frac{\gamma}{\gamma-1}} \left(\frac{\gamma+1}{2\gamma M^2 - (\gamma-1)}\right)^{\frac{1}{\gamma-1}} \tag{5}$$

Figure 5 indicates that the spacecraft approaches the subsonic region around 70 km, and it is assumed that conditions after the subsonic regime are constant–or the spacecraft has burned up. The latter is more likely since very high aerodynamic heating loads on the spacecraft (see Figure 6) occur between 70 km and 75 km altitude. The primary application of these reentry characterization plots is to inform design decisions for both the onboard sensors and the *Virtual Aperture* imaging system, which are discussed in the following sections.

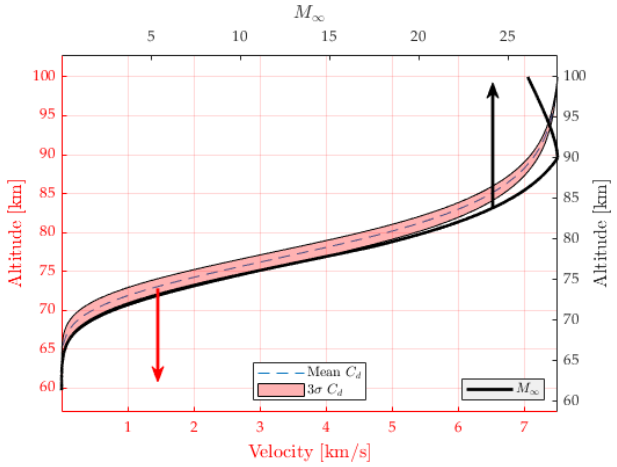

Figure 5: Velocity and freestream Mach number for a 1U CubeSat during atmospheric reentry. The C_d values were produced by assuming a Gaussian distribution to simulate tumbling. Shown here are the mean (dashed) and 3-σ drag coefficient region (shaded). The vehicle becomes sonic around 70 km and by this altitude the object has burned up. Arrows indicate associated plot axes.

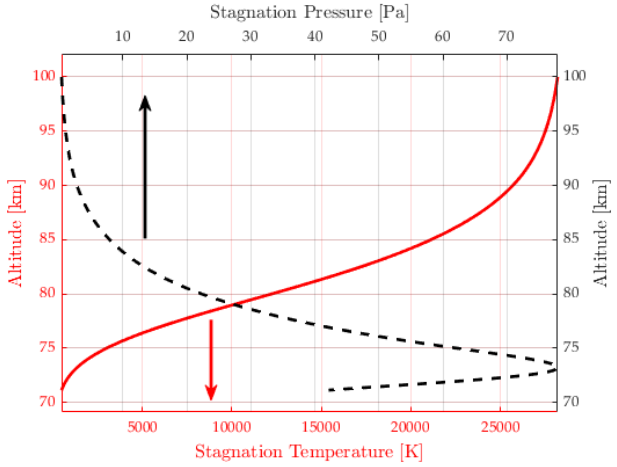

Figure 6: Stagnation temperature and pressure modeled at the forward-most facing part of the deorbiting spacecraft during reentry. Maximum heating and consequent burnup occurs around 75 km altitude, and around 70 km the vehicle (if any remains) goes subsonic and normal shock assumptions fail. Changes below this altitude are negligible and flow is treated as isentropic. Arrows indicate associated plot axes.

3. VÄMIAR-HÄRA

Virtual **Ä**perture **M**ultispectral **I**maging for **A**tmospheric **R**eentry studies using **H**igh-**Ä**ltitude **R**eflective Arrays. Very

commonly referred images of the AirBOS system capturing shockwaves off of two T-38 aircraft as imaged from an observer B-200 aircraft sets the stage on the feasibility of airborne measurements of supersonic flight. Similarly, re-entering vehicles and space debris provide excellent but infrequent and transient experimental facilities. Even so, with space commercialization and satellite constellation deployments on the rise, instances of deorbiting space debris due to collisions and other events are expected to increase [65–68]. The 136 flights of the Space Shuttle Transportation System (STS) provided much of the unclassified database on hypersonic boundary layers. These measurements on flight control implications on boundary layer behavior were made from aircraft that flew over the Gulf of Mexico and captured images of the vehicle both in space to confirm the integrity of thermal protection tiles on the vehicle surface, and hypersonic boundary layer thermal imaging as re-entry commenced. With the use of CubeSats, such studies can be extensively performed, and the CubeSat communities around the world are arming up to be the pioneers.

To create high-resolution thermal imagery, it is required to have impractically large apertures for radio telescopes to capture the infrared wavelengths. The demand for such large apertures is subverted by having several dish antennas of practical sizes. These regularly spaced parabolic antennas collectively form an equivalent of an exceptionally large aperture telescope. This concept of using discretely spaced interferometers is commonly known as synthetic or *Virtual Aperture*. Existing synthetic apertures are typically ground stations, like the Atacama Large Millimeter/Submillimeter (ALMA) observatory in Chile, demanding specific geographic and climatic conditions. Deriving analogies, in this section, we propose to use Glitter Belt architecture [69] to provide a virtual aperture for high-resolution multispectral imaging at higher altitudes. The Glitter Belt architecture was originally designed to reflect sunlight, thus reducing global warming, and anticipates fielding initial swarms of long-span, large aspect ratio ultralight reflective sheets (FLTs) supported at altitudes of 20 to 36.6 km. These swarms are designed to fly continuously 24 hours a day for several months during the summer. With the use of advanced manufacturing techniques, these have the potential to sustain high measurement payload capacity and data communications. The proposed idea revolves around using these reflector swarms as synthetic aperture imaging systems. The ultralight reflectors would be looking up into space and aimed at a CubeSat/orbital debris during reentry, enabling acquisition of the high-resolution multispectral imagery of spacecraft and debris during deorbiting and demising stages.

The initial application of a swarm of sensors looking upwards is to capture hypersonic boundary layer and wake characteristics of Low Earth Orbit vehicles immediately prior to and during re-entry over the southern Pacific and Indian ocean areas. The southern oceans, being remote with few shipping or airline routes, are the favored areas for disintegration and surface impact of orbital objects at end of life. The Glitter Belt Flying Leaf vehicles proposed by Komerath *et al.* [69] provide a unique set of platforms to perform imaging of re-entering vehicles. Very light wires can be integrated with the structural supports of the ultralight sheets to form antenna grids. Thus, much of the required mass budget of the imaging array may be met by vehicle structural elements. By combining several such vehicles in a swarm of suitable geometry, illustrated in Figure 7, it is possible to form a large, distributed telescope capable of responding to a broad spectrum of information from Space. Subsequent research will consider the characteristics of the flow fields around vehicles as they first encounter the atmosphere, and at later stages of descent. Future work will expand the system to look deeper into space to capture space weather phenomena and deep space objects in the IR regime. As shown in the Figure 7, the visibility of a reentry event from the farthest point would be limited by the line of sight above the horizon and future studies will explore optimal flight altitudes.

Eventually, we believe this synthetic aperture platform will produce high resolution data for temperature distribution of the spacecraft surface which will enable researchers to determine average temperature values for each location across the surface. This data will aid in our understanding of heat transfer rate to spacecraft during reentry and may lead to discoveries related to the entire state of the air in the vicinity of the surface at hypersonic velocities. The thermal images returned from the HYTHIRM project reveal obvious asymmetries in temperature distributions along the surface of the Shuttle Orbiter during reentry. Data extracted from this proposed synthetic aperture array could potentially describe the nature of these asymmetries.

The Glitter Belt architecture was originally designed to reflect sunlight, thus reducing global warming, and anticipates fielding initial swarms of long-span, large aspect ratio ultralight reflective sheets (FLTs) supported at altitudes of 20 to 30 km. These swarms are designed to fly continuously 24 hours a day for several months during the summer. With the use of advanced manufacturing techniques, these have the potential to sustain high measurement payload capacity and data communications. The proposed idea revolves around using these reflector swarms as synthetic aperture imaging systems. The ultralight reflectors would be looking up into space and aimed at a CubeSat/orbital debris during reentry, enabling acquisition of the high-resolution multispectral imagery of spacecraft and debris during deorbiting and demise stages.

Maximum Wavelength—Our first task is to establish a working understanding of the feasibility of a synthetic aperture with an effective diameter of 19,000 km to resolve a 1U CubeSat at the deorbit altitude of 120 km. Beginning with Wien's Displacement Law, we find the peak wavelength emitted by the blackbody source (in this case, a deorbiting 1U CubeSat).

Wien's Displacement Law:

$$\lambda_{peak} T = 2.898 \times 10^{-3} mK$$

Treating the CubeSat as a blackbody radiator with a maximum bow shock temperature of 2,800 K [70], we find that the maximum expected wavelength of the emission spectrum is $\lambda_{peak} = 1.04 \mu m$. Although the Planck blackbody spectrum (for the shock wave itself) at 2,800 K is a continuous distribution that includes other wavelengths, we note with satisfaction that this maximum wavelength output is well within the infrared.

Image Resolution—Most of our future work will consider sensors, pixel sizes, and resolution. At this point, we are interested in determining the general feasibility of the extremely large effective diameter for our "array telescope" made possible by our synthetic aperture architecture. We consider the curved sheets as mirror reflectors and utilize ray optics to make general conclusions about the proposed system. When forming an image using mirror surfaces, the ideal model of ray diagrams producing point-by-point images is not realistic. In reality, each "point" on the image formed by the mirror is

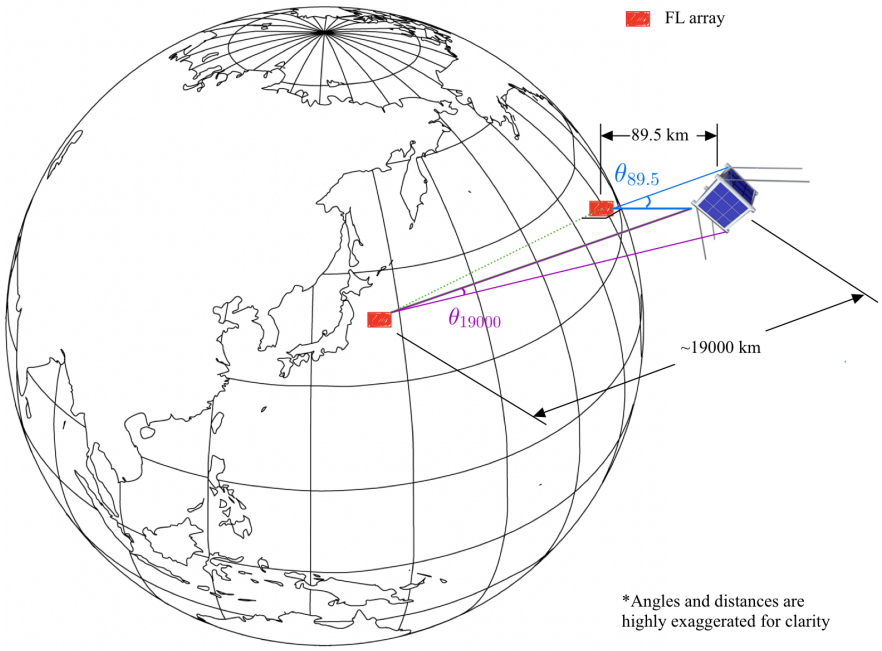

Figure 7: **Representative flight path and maximum viewing angle for the FLT high-altitude arrays (red). The θ values in this image represent angular separation between each edge of a face-on 1U CubeSat at the two extremes of the proposed system. Large distances between each high-altitude imaging system equate to a large virtual aperture optical system that predicts promisingly high resolution thermal imagery of hypersonic reentry objects.**

actually in the form of a diffraction pattern, usually circular in shape. These particular patterns are known as Airy disks, in honor of Sir George Airy (1801-1892), who first derived the expression for the intensity in the pattern [71]. We must assume that the resolution will be limited by diffraction of the light rays on their journey from the event to the flying sheet mirror surface, so we must employ Rayleigh's criterion to determine the minimum angular separation between two points on the object (the opposite ends of a small spacecraft when viewed face-on, in our case) that are just resolved.

Fraunhofer angular separation for a circular aperture is given by [72] as

$$sin\theta = 1.22\frac{\lambda}{D},$$

where θ is the angular separation between two points we wish to distinguish between, λ is the wavelength of the incident light, and D is the effective diameter of the synthetic aperture.

Resolving a Deorbiting 1U CubeSat—The angular separation between two sides of the front face of 1U CubeSat as viewed from a single FLT is obtained by using the small angle approximation, that is, $sin\theta \approx tan\theta$, for a right triangle with height equal to the straight-line distance (between the FLT and the CubeSat) and length equal to 10 cm.

For a conservative estimate, we consider the special case scenario when the CubeSat is directly overhead one of the FLT arrays such that the distance between one array and the satellite is 89.5 km, while the other FLT array sees a distance of roughly 19,000 km.

Solving for θ relative to the nearest array (shortest distance to the deorbit event), we find the angular resolution necessary to *barely resolve* two edges of a face-on 1U CubeSat.

$$\theta = tan^{-1}\left(\frac{0.10\ m}{89500\ m}\right)$$

$$\theta_{89.5km} = 64.0 \times 10^{-6} \text{ degrees} = 0.230 \text{ arcseconds}$$

Furthermore, we find that angular separation θ from 19,000 km is $\theta_{19{,}000km} = 0.00109$ arcseconds. These are the upper and lower bounds we might expect from the system when floating FLT arrays along the coast of Japan and the United States. We expect, of course, a major component of future work to be engineering the FLT systems flight dynamics and "stitching" the interferometric data together into a single useful image. These limits provide a starting point for our design and mission requirements.

Now that we have the upper and lower limits of resolution needed to resolve a 1U CubeSat in this configuration, we determine whether a Pacific Ocean-sized effective diameter aperture is adequate. Using Rayleigh's criterion for the minimum angular separation required to barely resolve two points, and using the wavelength determined earlier, we solve the diffraction equation directly and obtain the following approximate angular separation value:

$$\theta_{Synthetic} = \sin^{-1}\left(1.22\frac{\lambda_{max}}{D_{Synthetic}}\right)$$

$$= 3.83 \times 10^{-12} \text{ degrees} = 0.0137 \times 10^{-6} \text{ arcseconds}$$

The resolving power of such a synthetic aperture is *more than capable* of resolving a 1U CubeSat during reentry for both

the minimum and maximum expected distances, by a factor of 16.7×10^6 at the nearest approach and as small as 80000 $\times$ for the longest approach. Recall that these calculations depict the *minimum angular separation to just barely resolve two point objects,* a point we will take advantage of when designing the sensor system.

When considering a single FLT[2], we find that the maximum possible resolution is

$$\theta_{ResolutionFLT} = \sin^{-1}\left(1.22\frac{\lambda_{max}}{D_{FLT}}\right)$$

$$= 0.0795 \times 10^{-6} \text{ degrees} = 0.286 \times 10^{-3} \text{ arcseconds}$$

On the closest possible approach, the sensitivity required is 0.230 arcseconds. With a single FLT, it is theoretically possible to resolve a CubeSat with an angular separation as small as 0.286×10^{-3} arcseconds. Thus, on the closest approach, a single FLT would be able to resolve a CubeSat upon reentry by a factor of 800. For the farthest case, a single FLT at a distance of 19,000 km would still be able to resolve both sides of the CubeSat, but *only by a factor of 3.81*. It is important to recall here that the single FLT resolution is highly depenent upon the FLT span itself, which is, at this time, still an untested concept.

Optical Magnification— One structural configuration proposed by [62] is to form the thin sheet into a large-radius spherical mirror, creating a telescope-like array. From light ray optics and the dihedral geometry from Table 1, the magnification values for the system under consideration are represented in Figure 8.

To determine radius of curvature for each FLT, we considered four different dihedral angles consistent with common aircraft design: 2°, 3°, 4°, and 5°. The associated radius and focus for each configuration are given in Table 1.

Table 1: **Curved Sheet Configuration by Dihedral Angle**

Dihedral angle [°]	Radius [m]	Focus length [m]
2	458.37	229.19
3	305.58	152.79
4	229.18	114.59
5	183.34	91.67

Photon Intensity from Target and Observer Frames—Regardless of FLT configuration, future engineering considerations for design and implementation of this optical system will require intensity (power per unit area) values. We created the plots in Figure 8 in `MATLAB` using the Standard Atmosphere model and a T_s[3] value that varies over altitude as the satellite undergoes reentry. This information gives us an idea of the different expected intensity values predicted for different levels of the atmosphere, which is highly dependent upon blackbody temperature and ambient air temperature, T_∞, according to the Stefan-Boltzmann relationship.

[2]With a 2 degree dihedral angle, the diameter of a single FLT is 915 m. This is useful for our first architecture in which we treat the curved sheet as a spherical reflector.

[3]T_s is the temperature of the shock wave produced by the deorbiting object; the blackbody emission visible to the imaging system.

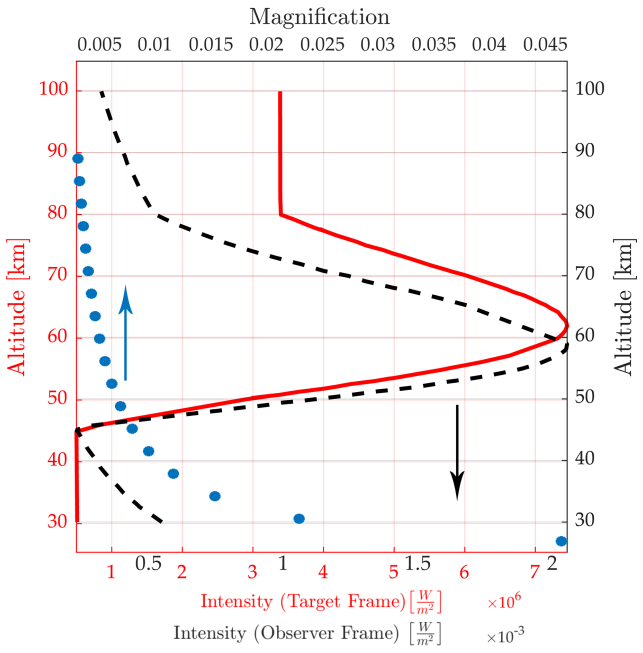

Figure 8: **(a) Lower x-axes. Thermal energy per unit area (Intensity) emitted by the reentry object (the Target) during atmospheric reentry from both the Target (solid; lowermost values on the x-axis) and Observer (dashed; arrow points to the uppermost values of the bottom x-axis), of the proposed high-altitude synthetic aperture optical system. Expected photon intensity values for the system will drive sensor and system architecture design. Note that the intensities sensed by the FLT array (the Observer) are on the order of mW/m^2. (b) Upper x-axis. Magnification (dotted; arrow points to x-axis) of the Target image seen from the Observer frame, treating the trailing sheets as spherical reflectors.**

Thermal energy per second per unit area (Intensity in $\frac{W}{m^2}$) with respect to altitude is shown in Figure 8 during reentry. Winter and Trumble's work forms the backbone of this plot, and constant values are assumed for the tip and tail of the distribution in the absence of empirical data points. The plots in Figure 8 relies heavily on the Stefan-Boltzmann law and the standard atmosphere model.

4. MEMS Pressure Sensor Array for Bluff Body Aerodynamics

This section focuses on the wireless pressure measurement capability with general applicability to small spacecraft; within the scope of current work, we focus on wind tunnel testing. The current state of standalone pressure sensor data collection systems for applications requiring wireless collection is typically limited to proprietary commercial solutions or one-off custom designs for specific use cases. Especially in ground testing where many solutions to measuring surface pressures on rotating test articles have been developed [73]. The approach presented here attempts to bridge the gap between the two by providing customizable architecture orders of magnitude cheaper than commercially available solutions. The key points throughout development were: 1) use open source hardware, when possible 2) use affordable and well-documented hardware 3) allow for adaptable application. The

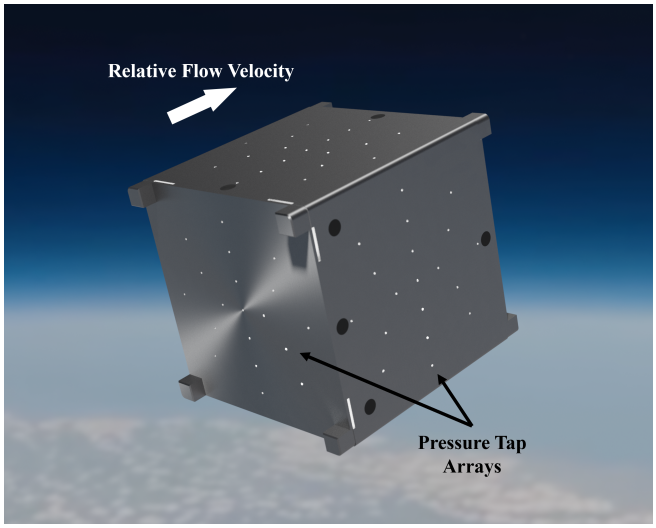

Figure 9: **1U CubeSat with pressure sensors flush mounted to the outer surface for aerodynamic data collection during atmospheric reentry.**

architecture for this type of pressure sensor system is suited for low-cost, small spacecraft-based aerodynamic measurements. An example 1U CubeSat is shown in Figure 9 with pressure taps on all outside surfaces.

Development for Low Subsonic Aerodynamics

The short-term intended application for the pressure sensor system is for rotating bluff bodies in the Cal Poly LWST, keeping in mind the long-term perspectives of studying the subsonic flow behind a normal shock. From a wind tunnel testing standpoint, direct pressure measurements are primarily limited to wired connections and pneumatic lines connecting from the test article to the pressure scanner (like Scanivalve, Validyne, and Kulite). Such a measurement system limits the direct pressure measurements to static conditions and in very specific cases like rotorcraft studies, slip rings are used. While wireless technology has increased in prominence in the telecommunication and 5G smart home appliance sectors, such a system is not absorbed well in the flow measurement technologies, especially in the aerospace sector. Such an effort was made in the circa 1970s [74] specific to pressure measurements on cylinders under unsteady flow conditions dictated by finite body rotation rates. However, this measurement system is not widely used, possibly due to the measurement uncertainties of the available sensors at the time. We propose to use digital commercially off-the-shelf (COTS) MEMS sensors configured to achieve desired spatial resolution for a wide variety of bluff objects. Within the current scope, we explore the system architecture of sensor array and their feasibility, thereby providing system performance and limitations for overall measurement time. The work addresses the achievable sampling rates and data writing speeds with the COTS accessible sensors and data acquisition systems. Thus, the resulting system is a standalone data collection system with onboard storage and battery, eliminating wires exiting the model. A diagram of the system can be seen in Figure 10. The aerodynamic measurement capability was made to capture low subsonic steady, quasi-steady, and low-frequency unsteady pressure fluctuations specific to low-speed wind tunnel applications.

Communication Protocol

The sensors available for use with the system originally were Honeywell ABP series I^2C piezoresistive silicon pressure sensors. The sensors are capable of a 2 kHz sampling rate with 12-bit temperature-compensated pressure output. Since first developing the system, Bourns BPS and All Sensors ELVH sensors have also been integrated into the system. In the future, Analog Microelectronics AMS 6915 sensors will be used to expand the capabilities of the system. The system design is designed for use with I^2C pressure sensors (I^2C is the type of digital communication protocol used for the sensors and microcontroller to transfer data). Such a system is suitable for short measurement distances, providing a good signal-to-noise ratio as compared to their analog counterparts, where background noise and inadequate electromagnetic shielding are problematic. With our main purpose of mounting several sensors at a finer spatial resolution, the board-mounted I^2C can be closely spaced and directly flushed to the measurement surfaces. The compressibility effects inside the pneumatic tubing leading to time lag or slower response rates are not a concern for flush-mounted sensors. The COTS sensors have a finite distance from the port location to the sensing element, and comprehensibility effects will not be significant within the sensor's frequency response of 2 kHz.

For each new sensor, a library must be developed to interpret the I^2C communication from the sensor to convert it into engineering units. While similar, the specific bit-by-bit output of the sensors is different but follows the general format as seen in Figure 11. The length of total communication between the master and slave devices is also varied; sensors capable of outputting temperature values (alongside pressures) will have communications two to three times longer than only pressure. All sensors used are pressure sensors of similar design but any I^2C device can be added easily. Serial Peripheral Interface (SPI) and analog devices are used for other functions of the system but additional sensors of either communication type can be added in addition to I^2C. The current focus of development is on expanding and testing I^2C pressure sensor capability, which will limit the scope of sensors and communication protocols covered in this paper.

One disadvantage to using exclusively I^2C pressure sensors is that many share I^2C addresses, even between brands, and are generally not re-programmable. The Analog Microelectronics sensors are the exception; multiplexers (MUX) are placed in the system between the sensor arrays and the microcontroller to expand the capability of the I^2C bus to read all available sensors. The multiplexer boards expand the I^2C bus from using a single sensor of a given address to eight per multiplexer. The multiplexers chosen have eight selectable addresses, allowing for 64 identical sensors before nesting. If additional sensors are required, the multiplexers can be nested to achieve theoretically unlimited sensors at the cost of significant bus speed reduction due to the added clocks per full sweep across all sensors, with the additional downside of increasing the number of pull-up resistors that can falsely put the system in logic High or Low states. The alternative is to use sensors such as the Analog Microelectronics AMS 6915 with reprogrammable addresses to achieve a theoretical maximum of 127 sensors on the microcontroller I^2C bus without a multiplexer in the loop to achieve higher data collection speeds. The system-level overview of the difference between the two configurations is depicted in Figure 10. Using and

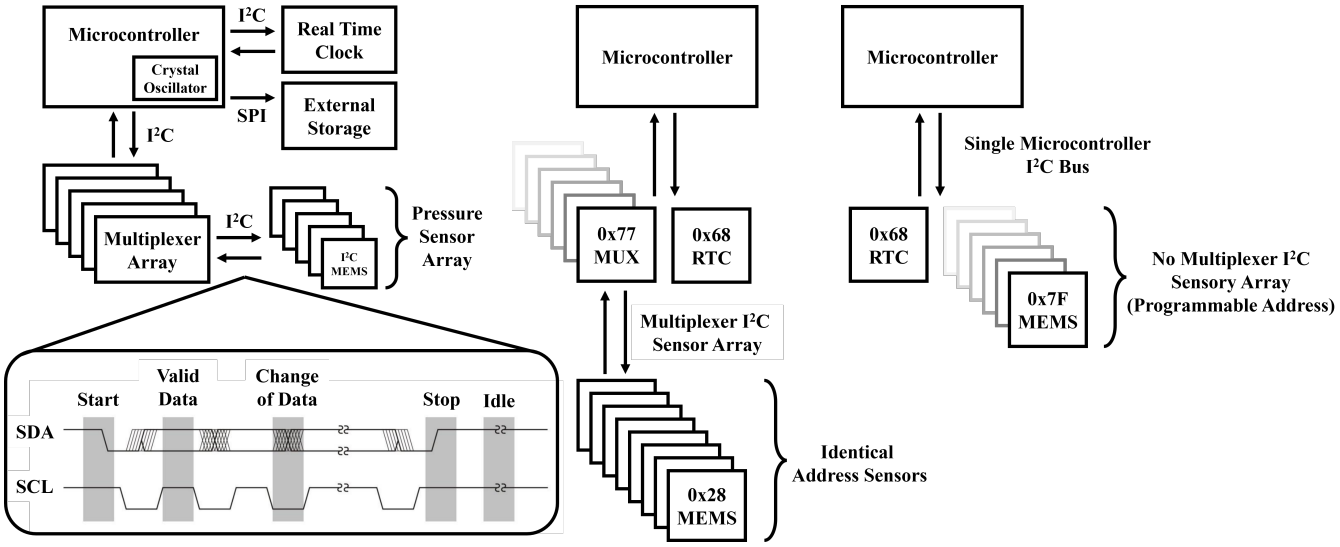

Figure 10: **Diagram of pressure sensor data acquisition system. Left: System component diagram with the communication protocol for each device. Middle: Device layout for device network with the use of multiplexers to allow for eight identical address pressure sensors per board. Right: Alternate device layout for I^{2}C device network using reprogrammable pressure sensors to eliminate multiplexers from the I^{2}C bus.**

analyzing the system with AMS 6915 sensors is not part of the scope of this paper. The implementation of the sensors is presently under development to quantify further differences between the use of multiplexers against unique address sensors. A select set of cases tested to measure time per sample difference between system configurations is shown in Table 2. It is clear that the overall response time increases from 4 ms to 20 ms for displaying data on a serial monitor versus writing onto an SD memory card. The limiting part of the current system for a select number of 6 sensors is the SD card write-up time, which brings the overall frequency response limited by 2 kHz for a single sensor down to 50 Hz. Future work will address efficient data writing methods on an SD card, possibly starting with binary file format recording raw sensor data, with data conversion occurring during post-processing. Figure 12 shows the sample results using board-mounted pressure sensors at steady state conditions.

Table 2: **Summarized tabulated data for overall system response time for operations related to (A) binary to calibrated pressure, (B) calibrated pressures to writing into a text file, (C) writing a string of random 14-bit decimal on Serial monitor or SD card.**

T(ms)	# of Sensors	Method	Note
22	6	SD	A
21	6	SD	A
20	6	SD	B
18	1	SD	A
9	6	Serial	A
9	6	Serial	B
4	6	Serial	-
1-2	1	Serial	A
1-2	0	Serial	$A + C$
1-2	0	Serial	C

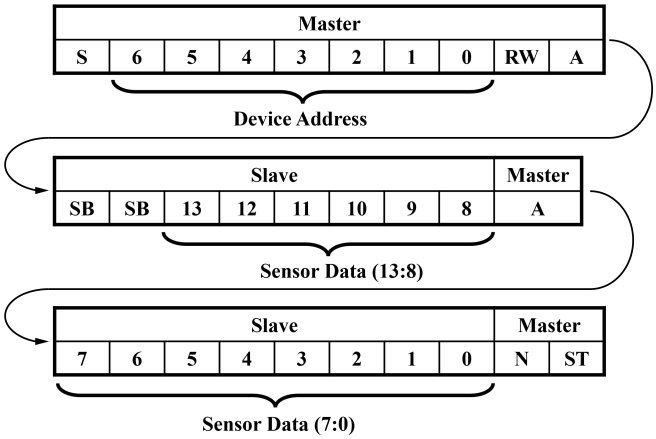

Figure 11: **Typical I^{2}C data exchange format for a 12-bit pressure sensor. The format is different between manufacturers so an individual interpreter for each sensor type is needed for data transformation.**

Hardware Selection

The microcontroller for data conversion and recording was chosen for cost, documentation, and ease of understanding specific to an undergraduate learning environment. There is an inherent bias in the decision-making process leaning toward open-source architectures. The full decision matrix for selecting Arduino can be seen in Figure 13. During the development of the system after selecting the Arduino Uno other boards have been researched and may be better suited to wind tunnel testing or spacecraft applications, such as the Teensy® 4.1, but were not known at the onset. There are difficulties with lifetime support for other boards meant for industrial applications as they heavily slow down the progress with the release of newer models and render the older ones obsolete (Texas Instruments MSP432EXP4111).

The additional instruments added to the microcontroller, through the use of an Arduino shield, are a real-time clock (RTC) and an SD card module. The built-in timing function

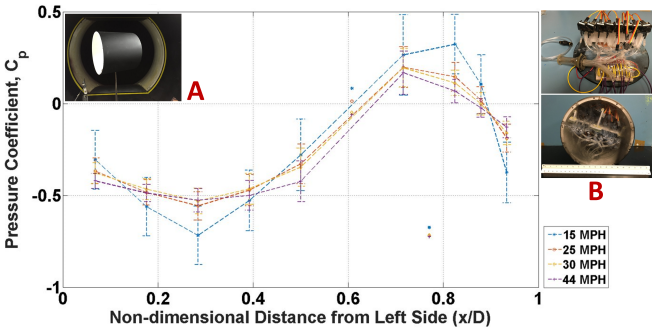

Figure 12: **Sample results showing the proof of concept by using board-mounted pressure sensors for capturing the pressures on the side surface of a cylinder (A) for low-speed testing. Tests were performed under steady-state conditions with the sensor array lined along the diameter of the side plate (B).**

Criteria	Weight	Texas Instruments MSP432EXP4111	Texas Instruments MSP432E4	Arduino Uno Rev3	Arduino Uno WiFi Rev2	Ruggeduino-SE ST	Raspberry Pi 3 Model A+
Product							
Cost	1	5	2	4	2	1	3
Documentation	4	1	2	5	4	4	5
Durability	3	2	2	2	2	5	2
Reliability	4	4	4	2	2	4	2
I2C Support	3	3	3	2	2	2	1
Ease of Accessibility	5	1	1	5	4	4	2
IDE	2	2	2	4	4	4	4
MATLAB / Python	3	0	0	5	5	5	5
Product Lifecycle Duration	4	0	1	5	3	4	3
Overall Weighted Score		**49**	**54**	**112**	**93**	**113**	**85**

Figure 13: **Decision matrix comparison between circuit board options during early system development. The leading choice at the time was Arduino Uno and the similar Ruggeduino-SE ST.**

of the Arduino is sufficient for recording timing between pressure sensor samples but cannot be synchronized to other data collection systems. The RTC allows for time synchronization but only for aligning data files to the same sampling period, not for exact synchronization. For the pressure data to be synchronized with external data sequences, such as an encoder, an alternate timing source to create a zero point in both data sets would be required. This is necessary because of timing limitations when originally synchronizing the RTC, a time delay is present during compilation of a few milliseconds depending on system performance. The SD card is used for data collection of potentially large data sets over hours of data recording for slow rotations or many module attitudes. In the future, SRAM modules and other storage devices could be integrated for faster write speeds, reduced size, or more durable construction. Currently, writing data onto the SD card is a significant bottleneck to the system performance and maximum data collection rate.

The pressure sensors currently in use would not be suitable for flight conditions, as they are designed for dry gasses with limited temperature range—ideal for ground testing facilities. A different array of pressure sensors is required for spacecraft reentry applications, although when designed for harsh conditions, the sensors' capabilities should not be significantly altered. The individual sensor's response rate of 2 kHz brings hope for performing unsteady pressure measurements wherein resolving the temporal scales of large-scale structures from the bluff bodies is achievable. The cost of the system, including sensors, is a few hundreds of dollars (USD) depending on the number of sensors used; excluding sensors, the base system is less than $100 USD. Compared to commercially available solutions for industrial applications, the total cost is one to two orders of magnitude cheaper. The low cost and open source design allows the system to be used in academic facilities for student use or in sacrificial applications.

5. Conclusions

The paper explores the system architecture for using small spacecraft as a platform for bluff body aerodynamics. It explores the technology gaps within the measurement technology, like the wireless data acquisition for ground testing and flight testing specific to the aerodynamic characterization of large-scale flow features stemming from finite-sized bluff bodies. Most importantly, it sheds light on how high-altitude aerial systems can be used as a platform for improving telemetry and optical diagnostics of reentering spacecraft. This combination of onboard diagnostics followed by multispectral imaging shows pathways for better managing space debris, improved capabilities for terrestrial and astronomy observations, and technology advancement in targeted reentry studies.

The authors have taken the first step toward developing a very high resolution, very high-altitude long endurance *Virtual Aperture* system that will outperform current similar ground and space-based systems in resolution, data collection, and mobility. Concept studies-level research was undertaken to address the increasing need for orbital debris and reentry object tracking, management, visualization, and study using novel high-altitude optical assets. A framework for possible system architecture was proposed, and expected flow parameters for a 1U CubeSat during reentry were evaluated. The purpose behind developing aerial multispectral imaging capability is to establish a baseline for feasibility studies concerned with studying deorbiting objects as a testbed for hypersonic research and bluff body aerodynamics that respects real-environment effects that cannot be easily produced in a wind tunnel setting. The target IR band(s) for visualizing hypersonic flow over a body during atmospheric reentry fall in the IR range, which accords with the predicted heating and emission spectrum of a blackbody. The intensity maps show the feasibility studies and act as a starting point for designing suitable sensor arrays to capture irradiation of the order of mW/m^2 at an imaging flight altitude of 30 km. It is assumed that the simulated breakup occurs around 60-70 km due to aero-thermal loads and is limited to thermally perfect gas

assumptions while respecting the vibrational modes.

Velocity and mach relations over a 3σ drag coefficient were developed for a "roadmap" of the flight reentry envelope to map the relative distances between the reentry spacecraft and the high-altitude aerial systems.The angular positions of two surfaces of a face-on CubeSat at the beginning of reentry ($\approx$120 km) are 64.0×10^{-6} degrees straight up[4]and 0.302×10^{-6} degrees as seen from across the Pacific Ocean as seen by the FLT array[5]. A Pacific Ocean-wide *Virtual Aperture* provides an angular resolution of $= 3.83 \times 10^{-12}$ degrees, which is more than able to resolve a CubeSat at 120 km by a factor of 16.7×10^6 at the closest approach and 80000 at the furthest, with no dependency upon the individual FLT flight configuration. Photon intensities at the receiver (Observer) expected variability as the spacecraft descends through the ambient air temperature and pressure gradient layers with intensities at the receiver that range between 0.00025 and 0.0021 $\frac{W}{m^2}$. These metrics are useful for sensor and instrumentation design in future work.

Lastly, the system architecture for COTS board-mounted pressure sensors is explored as a viable alternative for unsteady pressure measurements for low-speed wind tunnel testing. The sensors themselves have a response rate of 2 kHz but the overall system response is limited to 50 Hz for writing data to a memory card. Several aspects like reliability, ease of accessibility, and life cycle support were critical factors in choosing the various components. It was also discussed how digital sensors with the same addresses (or programmable addresses) synchronized with an RTC could be used for creating pressure sensor arrays to resolve unsteady large-scale pressure fluctuations stemming from bluff bodies. The approach of using onboard sensor arrays for spacecraft as a test bed for bluff body aerodynamics combined with high-altitude virtual aperture technique shows opportunistic avenues for technology development for targeted reentry studies.

ACKNOWLEDGMENTS

The authors thank Dr. Narayanan Komerath and Taksha Institute for providing fixed-wing model geometries for high-altitude applications. The Authors wish to thank Professor Greg Adams, formerly of the U.S. Naval Research Laboratory, for his invaluable expertise and thoughtful suggestions that helped synthesize this concept into a logical scientific flow.

REFERENCES

[1] J. Gerrard, "The Mechanics of the Formation Region of Vortices Behind Bluff Bodies," *Journal of Fluid Mechanics*, vol. 25, pp. 401–413, 1966.

[2] R. King, "A Review of Vortex Shedding Research and Its Application," *Ocean Engineering*, vol. 4, pp. 141–171, 1977.

[3] F. H. Barnes and I. Grant, "Vortex shedding in unsteady flow," *Journal of Wind Engineering and Industrial Aerodynamics*, vol. 11, pp. 335–344, 1983.

[4] P. Bearman and T. Morel, "Effect of free stream turbulence on the flow around bluff bodies," *Progress in aerospace sciences*, vol. 20, no. 2, pp. 97–123, 1983.

[5] K. Koenig and A. Roshko, "An experimental study of geometrical effects on the drag and flow field of two bluff bodies separated by a gap," *Journal of Fluid Mechanics*, vol. 156, no. 1, p. 167, 1985.

[6] P. Bearman and N. Tombazis, "The effects of three-dimensional imposed disturbances on bluff body near wake flows," *Journal of Wind Engineering and Industrial Aerodynamics*, vol. 49, pp. 339–350, 1993.

[7] Y. Nakamura, "Bluff-body aerodynamics and turbulence," *Journal of Wind Engineering and Industrial Aerodynamics*, vol. 49, pp. 65–78, 1993.

[8] M. Matsumoto, "Vortex Shedding of Bluff Bodies: A Review," *Journal of Fluids and Structures*, vol. 13, pp. 791–811, 1999.

[9] J. Bentley and J. Mudd, "Vortex shedding mechanisms in single and dual bluff bodies," *Flow Measurement and Instrumentation*, vol. 14, pp. 23–31, 2003.

[10] A. Forbes, S. Pirau, B. Liberi, V. Raghav, and N. Komerath, "Testing-based approach to determining the divergence speed of slung loads," in *Proceedings of the 70th American Helicopter Society Forum*, May 2014.

[11] M. Mokry, J. Digney, and R. Poole, "Doublet-panel method for half-model wind-tunnel corrections," *Journal of Aircraft*, vol. 24, no. 5, pp. 322–327, 1987.

[12] N. Komerath, N. Hiremath, D. Shukla, J. Robinson, A. Jha, and A. Palaniappan, "Aerodynamic loads on arbitrary configurations: Measurements, computations and geometric modeling," SAE Technical Paper, Tech. Rep., 2017.

[13] A. Pelletier and T. J. Mueller, "Low reynolds number aerodynamics of low-aspect-ratio, thin/flat/cambered-plate wings," *Journal of Aircraft*, vol. 37, no. 5, pp. 825–832, 2000.

[14] J. Pinier, J. L. Hanke, and W. G. Tomek, "Ares i aerodynamic testing at the boeing polysonic wind tunnel," *Journal of Spacecraft and Rockets*, vol. 49, no. 5, pp. 853–863, 2012.

[15] S. Pirau, B. Liberi, N. Barbely, and N. Komermath, "Aerodynamic load maps of bluff bodies: Measurements and diagnostics," *Journal of Mechanical Science and Technology*, 2009.

[16] V. Raghav, R. Mantri, N. Komerath, and M. Smith, "Study of factors driving pitch, roll and yaw coupling in bluff body aerodynamics," in *AIAA Applied Aerodynamics Conference*, 2011.

[17] S. Pirau, V. Raghav, A. Forbes, B. Liberi, and N. Komerath, "Efficient airload determination for bluff body aeromechanics," in *Proceedings of the ASME 2014 International Mechanical Engineering Congress & Exposition*, November 2014.

[18] B. Liberi, S. Pirau, V. Raghav, and N. Komerath, "Determination of slung load divergence speed using airload measurement and simulation," in *Proceedings of the ASME 2014 International Mechanical Engineering Congress & Exposition*, ser. ASME Paper, no. IMECE2014-38260, November 2014.

[19] N. Komerath, S. Pirau, and B. Liberi, "Generalized prediction of bluff-body aerodynamic load maps," in *Proceedings of the ASME-JSME-KSME Joint Fluids*

[4] Or, the shortest distance

[5] Or, 0.230 arcseconds and 0.00109 arcseconds, respectively.

Engineering Conference, ser. Paper, no. AJK2015-FED, Seoul, Korea, July 2015.

[20] N. Motahari, F. D'Turbeville, N. Hiremath, and N. Komerath, "Airload maps of vehicle shapes at arbitrary attitude," in *Proceedings of the SAE Aerotech Conference*, ser. Paper, no. 2015-01- 15ATC-0198, Seattle, WA, September 2015.

[21] B. Liberi, C. Ton, and N. Komerath, "Divergence speed prediction for practical slung load shapes," in *Proceedings of the ASME-JSME-KSME Joint Fluids Engineering Conference*, ser. Paper, no. AJK2015-27543, Seoul, Korea, July 2015.

[22] N. Komermath, V. Raghav, and N. Hiremath, *Aerodynamic Loads On Arbitrary Shapes*. SCV Inc, 2016.

[23] N. Komerath, N. Hiremath, and D. Shukla, "Testing-based approach to determining the divergence speed of slung loads," *Aerospace*, vol. 5, no. 1, 2018. [Online]. Available: https://www.mdpi.com/2226-4310/5/1/24

[24] Q. Cockrell and N. Hiremath, "Development and integration of continuous load and position measurement for quasi-steady flows," in *Proceedings of the ASME 2023, International Mechanical Engineering Congress and Exposition*. ASME, 2023, pp. IMECE2023–113 814.

[25] M. Thomas, D. Pandey, and J. Nguyen, "Flow Characteristics of the Renovated Cal Poly 3 x 4 ft Subsonic Wind Tunnel," Cal Poly, Technical Report, September 2011.

[26] S. F. Hoerner, *Fluid-dynamic drag: practical information on aerodynamic drag and hydrodynamic resistance*. Hoerner Fluid Dynamics Midland Park, NJ, 1965.

[27] S. F. Hoerner and H. V. Borst, "Fluid-dynamic lift: practical information on aerodynamic and hydrodynamic lift," 1985.

[28] C. Norberg, "An experimental investigation of the flow around a circular cylinder: influence of aspect ratio," *Journal of Fluid Mechanics*, vol. 258, no. 1, pp. 287–316, 1994.

[29] A. Roshko, "Experiments on the flow past a circular cylinder at very high reynolds number," *J. Fluid Mech*, vol. 10, no. 3, pp. 345–356, 1961.

[30] R. Windsor, "Wind tunnel tests of two models of rectangular containers," Glenn Martin Wind Tunnel, University of Maryland, College Park, MD, USA, Report 573, January 1970.

[31] D. Sheldon and J. Pryor, "Study in depth of a single point and two point lateral and tandem suspension of rectangular box loads," The Royal Military College of Science, Technical Note AM 38, May 1973.

[32] L. Cicolani and G. Kanning, "A comprehensive estimate of the static aerodynamic forces and moments of the 8- by 8- by 20-foot cargo container. , nasa, may." NASA, Tech. Rep. 89433, 1987.

[33] M. Zdravkovich, V. Brand, G. Mathew, and A. Weston, "Flow past short circular cylinders with two free ends," *Journal of fluid mechanics*, vol. 203, no. 1, pp. 557–575, 1989.

[34] M. Zdravkovich, A. Flaherty, M. Pahle, and I. Skelhorne, "Some aerodynamic aspects of coin-like cylinders," *Journal of Fluid Mechanics*, vol. 360, no. 1, pp. 73–84, 1998.

[35] A. Rosen, S. Cecutta, and R. Yaffe, "Wind Tunnel Tests of Cube and CONEX Models," *Technion Institute of Technology, Dept. of Aerospace Engineering, TAE*, vol. 844, 1999.

[36] N. Motahari, N. Hiremath, D. Shukla, B. Liberi, N. Thorell, and N. Komerath, "Generalized airloads prediction for bluff bodies transported as slung loads," in *ASME International Mechanical Engineering Congress and Exposition*, vol. 57557. American Society of Mechanical Engineers, 2015, p. V012T15A026.

[37] S. Szepessy and P. Bearman, "Aspect ratio and end plate effects on vortex shedding from a circular cylinder," *Journal of Fluid Mechanics*, vol. 234, no. 1, pp. 191–217, 1992.

[38] N. Hiremath, D. Shukla, A. Pandey, J. W. Gregory, and N. Komerath, "Pressure field of a yawed aspect ratio 1 circular cylinder," in *ASME International Mechanical Engineering Congress and Exposition*, vol. 58424. American Society of Mechanical Engineers, 2017, p. V007T09A021.

[39] S. Komatsu and H. Kobayashi, "Vortex-induced oscillation of bluff cylinders," *Journal of Wind Engineering and Industrial Aerodynamics*, vol. 6, pp. 335–362, 1980.

[40] B. Lee, "Some Observations of the Effect of Aspect Ratio on the Influence of Turbulence on the Drag of Rectangular Cylinders," *Journal of Wind Engineering and Industrial Aerodynamics*, vol. 33, pp. 107–111, 1990.

[41] C. S. Wells Jr., "Effects of freestream turbulence on boundary-layer transition." *AIAA Journal*, vol. 5, no. 1, pp. 172–174, 1967.

[42] C. Wei and J. Chang, "Wake and base-bleed flow downstream of bluff bodies with different geometry," *Experimental Thermal and Fluid Science*, vol. 26, pp. 39–52, 2002.

[43] M. Pastoor, L. Henning, B. R. Noack, R. King, and G. Tadmor, "Feedback shear layer control for bluff body drag reduction," *Journal of fluid mechanics*, vol. 608, no. 1, pp. 161–196, 2008.

[44] T. W. Jones, C. B. Lunsford, and S. S. Graves, "Design and development of a real-time model attitude measurement system for hypersonic facilities," in *43rd AIAA Aerospace Sciences Meeting*, 2005.

[45] A. Cassell, P. Wercinski, B. Smith, B. Yount, O. Nishioka, and C. Kruger, "Adept sounding rocket one flight test overview," in *AIAA Aviation 2019 Forum*, 2019, p. 2896.

[46] A. M. Korzun, S. Dutta, R. D. McDaniel, C. D. Karlgaard, and J. A. Tynis, "Aerodynamics for the adept sr-1 flight experiment," in *AIAA Aviation 2019 Forum*, 2019, p. 2897.

[47] J. R. Cruz and J. S. Green, "Subsonic dynamic testing of a subscale adept entry vehicle," in *AIAA Aviation 2019 Forum*, 2019, p. 2898.

[48] I. Sakraker, E. Umit, T. Scholz, P. Testani, G. Baillet, and V. Van der Haegen, "Qarman: An atmospheric entry experiment on cubesat platform," in *8th European Symposium on Aerothermodynamics for Space Vehicles*, no. 1, 2015.

[49] D. Masutti, E. Trifoni, E. Umit, A. Martucci, A. Denis, C. Purpura, T. Scholz, G. Ceglia, P. Testani, I. Sakraker *et al.*, "Qarman re-entry cubesat: preliminary results of scirocco plasma wind tunnel testing," in *15th interna-*

tional planetary probe workshop short course—small satellites: an emerging paradigm for bold planetary exploration. Boulder CO, 2018.

[50] C. Miccoli, A. Turchi, P. Schrooyen, D. D'Ambrosio, and T. Magin, "Detailed modeling of cork-phenolic ablators in preparation for the post-flight analysis of the qarman re-entry cubesat," *Aerotecnica Missili & Spazio*, vol. 100, pp. 207–224, 2021.

[51] W. R. Coulton, M. S. Madhavacheril, A. J. Duivenvoorden, J. C. Hill, I. Abril-Cabezas, P. A. Ade, S. Aiola, T. Alford, M. Amiri, S. Amodeo *et al.*, "The atacama cosmology telescope: High-resolution component-separated maps across one-third of the sky," *arXiv preprint arXiv:2307.01258*, 2023.

[52] T. Horvath, D. Tomek, S. Splinter, J. Zalameda, P. Krasa, R. Schwartz, D. Gibson, A. Tietjen, and K. Berger, "The hythirm project: flight thermography of the space shuttle during hypersonic re-entry," in *48th AIAA Aerospace Sciences Meeting Including the New Horizons Forum and Aerospace Exposition*, 2010, p. 241.

[53] D. Gibson, T. Spisz, J. Taylor, J. Zalameda, T. Horvath, D. Tomek, A. Tietjen, S. Tack, and B. Bush, "Hythirm radiance modeling and image analyses in support of sts-119 and sts-125 and sts-128 space shuttle hypersonic re-entries," in *48th AIAA Aerospace Sciences Meeting Including the New Horizons Forum and Aerospace Exposition*, 2010, p. 244.

[54] R. Schwartz, H. Verstynen, J. Gruber, S. Splinter, D. Hensley, T. Horvath, A. McCrea, T. Oram, K. Berger, and R. Kerns, "Remote infrared imaging of the space shuttle during hypersonic flight: Hythirm mission operations and coordination," in *42nd AIAA Thermophysics Conference*, 2011, p. 3326.

[55] N. Komerath, S. Hariharan, D. Shukla, S. Patel, V. Rajendran, and E. Hale, "The flying carpet: Aerodynamic high-altitude solar reflector design study," SAE Technical Paper, Tech. Rep., 2017.

[56] N. Komerath, D. Shukla, S. Hariharan, S. Patel, and N. Hiremath, "Tradeoff study of high altitude solar reflector concepts," SAE Technical Paper, Tech. Rep., 2017.

[57] M. C. Smith-Pierce, Y. C. Charoenboonvivat, D. Shukla, and N. M. Komerath, "High altitude aerodynamic reflectors to counter climate change," in *2018 Applied Aerodynamics Conference*, 2018, p. 3963.

[58] N. Komerath, R. Deepak, and A. Deepak, "An aerospace approach to counter climate change," in *Proceedings of the MIT applied energy symposium MIT A+ B co-organized with Harvard*. Applied Energy MIT, Cambridge, MA, USA, 2022.

[59] R. D. Narayanan Komerath and A. Deepak, "Stem opportunities in flight testing sunlight reflector ultralights," in *New Achievements in Unmanned Systems: International Symposium on Unmanned Systems and the Defense Industry 2021*. Springer Nature, 2023, p. 57.

[60] N. M. Komerath and R. Deepak, "A reversible mid-stratospheric architecture to reduce insolation," *Applied Energy*, vol. 348, p. 121575, 2023.

[61] N. Komerath, S. Meti, N. Hiremath, and R. Ramachandran, "Wildfire detection using hale meteorology vehicles," in *2023 4th IEEE Global Conference for Advancement in Technology (GCAT)*. IEEE, 2023, pp. GCAT2023–876.

[62] J. Self and N. Hiremath, "Virtual Aperture Multispectral Imaging for Atmospheric Reentry Studies Using High-Altitude Reflective Arrays," in *Presented at the AMS Annual Meeting. American Meteorological Society*, Dec 2021.

[63] ——, "Virtual Aperture Multispectral Imaging for Atmospheric Reentry Studies Using High-Altitude Reflective Arrays," in *AIAA Region VI Student Paper Conference*, Apr 2022.

[64] ——, "Virtual Aperture Multispectral Imaging for Atmospheric Reentry Studies Using High-Altitude Reflective Arrays," in *Presented at 2023 AAAS S-STEM Scholars Meeting., Washington DC*, Sep 2023.

[65] R. Walker, P. Stokes, J. Wilkinson, and G. Swinerd, "Long-term collision risk prediction for low earth orbit satellite constellations," *Acta Astronautica*, vol. 47, no. 2-9, pp. 707–717, 2000.

[66] P. H. Krisko, "The predicted growth of the low-earth orbit space debris environment—an assessment of future risk for spacecraft," *Proceedings of the Institution of Mechanical Engineers, Part G: Journal of Aerospace Engineering*, vol. 221, no. 6, pp. 975–985, 2007.

[67] A. Rossi and G. Valsecchi, "Collision risk against space debris in earth orbits," *Celestial Mechanics and Dynamical Astronomy*, vol. 95, no. 1, pp. 345–356, 2006.

[68] D. J. Kessler, "Collisional cascading: The limits of population growth in low earth orbit," *Advances in Space research*, vol. 11, no. 12, pp. 63–66, 1991.

[69] N. Komerath, A. Sharma, R. Deepak, and A. Deepak, "Glitter Belt Global Measurement System: Indian Ocean Component Preparation," in *2021 International Conference on Electrical, Computer, Communications and Mechatronics Engineering (ICECCME)*. IEEE, 2021, pp. 1–6.

[70] M. Winter and G. Herdrich, "Spectroscopic observation of the stardust re-entry in the near uv," in *39th AIAA Thermophysics Conference*, 2007, p. 4050.

[71] H. D. Young, R. A. Freedman, and A. L. Ford, *University Physics with Modern Physics Technology Update*. Pearson Education, 2013.

[72] F. L. Pedrotti, L. M. Pedrotti, and L. S. Pedrotti, *Introduction to optics*. Cambridge University Press, 2017.

[73] M. Miller, "Approaches to measure the surface pressures on spinning bodies," 10 2016.

[74] M. C. Miller, "Surface pressure measurements on a spinning wind tunnel model," *AIAA Journal*, vol. 14, no. 12, pp. 1669–1670, 1976. [Online]. Available: https://doi.org/10.2514/3.61510

BIOGRAPHY

Nandeesh Hiremath *received his Ph.D. degree in Aerospace Engineering from Georgia Tech. He is currently an Assistant Professor and Principal Director in the Applied Experimental Fluids Group at California Polytechnic State University, San Luis Obispo. With his budding research group, his contributions are aimed at advancing experimental techniques for studying bluff body aerodynamics, with specific interests in space applications.*

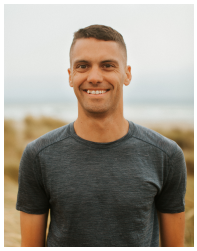

Justin Self *is a fourth-year undergraduate student in the Aerospace Engineering program at Cal Poly. He plans to complete his B.S. in Aerospace Engineering with a minor in Physics in 2024 and his masters degree in Aerospace Engineering by early 2025. Justin has been part of Dr. Hiremath's Applied Experimental Fluids research group since 2021, where he is currently working to develop a high-altitude synthetic aperture multispectral imaging system for atmospheric reentry studies.*

Nathan Eller *is currently a dual degree master's student in Aerospace Engineering at Cal Poly. He plans to complete his degree in 2024. Nathan has been working with Dr. Hiremath on the development of a pressure sensor system for rotating test articles in the Cal Poly Low-Speed Wind Tunnel. He has also interned at NASA Ames Fluid Mechanics Laboratory, assisting with wind tunnel CFD integration and acoustics analysis.*